Journal of Optoelectronics and Advanced Materials Vol. 1, No. 1, March 1999, p. 17-26

INTERFEROMETRIC DEVICES FOR INTEGRATED OPTICS REMOTE SENSOR SYSTEMS

H. Porte[a], W. Elflein, J.P. Goedgebuer
Laboratoire d'Optique P.M. Duffieux, UMR CNRS 6603
[a]Université de Franche-Comté, Institut des Microtechniques
F-25030 Besançon, Cedex France

This paper reports some recent results obtained in the field of integrated optics technology applied to coherence modulation sensor systems and proposes several examples of integrated Mach-Zehnder interferometers featuring optical delays of some tens to some hundred of micrometers, each of them being specifically designed for one sensing application. The first device is based on the use of lithium niobate technology. This electrooptic device can be used in the demodulation process of the sensor system which uses an electronic feedback to produce a linear phase tracking of the signal supplied by the sensor and yields to a remote sensor system, able to read the phase variations produced by any interferometric sensor. This system is applied to a gas sensing operation involving a second device integrated in glass by using an ion exchange process (K^+-Na^+). The phase variations are produced here by the interaction of the evanescent wave of the guided light with a thin polymeric layer. The refractive index variation of the latter is proportional to the concentration of absorbed gas, resulting in a chemical sensor, able to detect and measure the concentration in air of organic gases. The last example of integrated optical device uses the silicon technology. The aim is to realize a micromachined pressure optical sensor. Under one waveguide arm, a set of membranes is etched by anisotropic etching using KOH. The variations of optical path delays are obtained here by deformation of the membranes submitted to pressure variations.

(Received September 23, 1998; accepted November 27, 1998)

1. Introduction

The application of optical fibers in sensor systems has been investigated for many years, using them as a transmission support, but also for their capability to sense various physical parameters intrinsically [1]. Singlemode fibers become highly sensitive phase transducers for these parameters when used in an interferometric configuration. Several problems need careful attention in such sensor systems in order to achieve good performance. First of all, although all-fiber interferometers feature a high sensitivity, their output is a non-linear cosine function of the phase which can therefore not be read directly and a demodulation process is required to retrieve the original signal. An other drawback of all-fiber interferometers is the difficulty to separate different parameters (e.g. pressure and temperature) at the output.

Coherence modulation is based on the use of a CW broadband source (BBS) with a low-coherence radiation, and interferometers whose optical path-difference (OPD) is larger than the coherence length. Coherence modulation [2-4], when coupled to integrated optics technology is an attractive way to solve a part of the problems mentioned previously. One advantage of coherence modulation is the possibility to determine the amplitude and the sign of the fringe displacement which is proportional to the signal applied to the sensor. Therefore, the demodulation can be unambiguous, even if the phase variation of the signal is larger than π. The solution consists to detect directly the output power with a receiving interferometer tracking the OPD to be measured.

However, as most of the demodulation interferometers previously reported up to the present are all-fiber devices [5], they can suffer from temperature and mechanical instabilities. The

development of superluminescent diodes (SLD) whose coherence length does not exceed some tens of microns makes the use of electrically driven integrated optics transducers possible. These compact devices are inherently more stable and reliable than the large path-imbalanced (>1m) all-fiber interferometers required for laser sources with long coherence length. A system based on the use of integrated optics modulators is quasi temperature independent.

We describe first in this paper a sensor system dedicated to the measurement of concentration of organic gases. This system is based on the use of coherence modulation and allows a remote interferometric measurement. Two different integrated optics technologies are required in a complementary way. Integrated optics in glass is used to realize the sensor itself, whereas lithium niobate technology is used for the demodulation process which performs an active phase read-out [6,7]. The sensor uses a polymer material whose refractive index varies with the gas concentration, and thus modifies the characteristics of the evanescent part of the wave propagating in the glass waveguide.

Then, we investigate theoretically and experimentally the principle of a micromachined pressure sensor integrated in silicon [8-10]. The optical part of the sensor consists of an imbalanced Mach-Zehnder waveguide interferometer. The sensing part of the device consists in a set of membranes obtained by anisotropic etching of the back face of the substrate under the reference arm. The pressure variations applied to the membrane induce a geometrical deformation of the waveguide arm and modify the optical path-difference between the arms. The non linear variation of the phase versus the applied pressure is obtained from the spectral analysis of the channeled spectrum transmitted by the interferometer. The static optical path-delay introduced between the arms allows the sensor to be introduced in a coherence modulation scheme, which can results in a remote sensor system, involving an active demodulation.

2. Gas sensor system

2.1. Description of the system and principle of operation

Integrated optics technology allows solid-state interferometric structures to be realized that are more robust and reliable and whose response is more selective than fiber sensors. Another advantage is that the interaction of evanescent waves with a material deposited directly onto the waveguide is easily realized since the optical waveguides are generally located at the substrate surface [11,12].

Fig. 1 shows the setup of the gas sensor system which is based on the former principle. This system includes an optoelectronic central processing unit (OECPU) and an in-line gas sensor connected to the former by optical fiber. The OECPU contains a short coherence length optical source. The latter is a superluminescent diode of optical power P_o=0.5 mW emitting at λ_o=1280 nm, and of the spectral width $\Delta\lambda$=50 nm. Thus, the coherence length is $\ell_c=\lambda_o^2/\Delta\lambda$=32 μm. At the measurement site, a Mach-Zehnder interferometer integrated in a glass substrate is used as a sensor.

The two arms of the interferometer are of different length L_1 and L_2. Here, any wave packet of coherence length ℓ_c, emitted by the continuous wave broadband source (BBS) is divided in two wave packets. At the output of the interferometer, these packets are separated by a fixed optical delay $\delta_o=n_{eff}(L_2-L_1)$, δ_o being larger than the coherence length ℓ_c. Here, n_{eff} is the effective index of the guided mode.

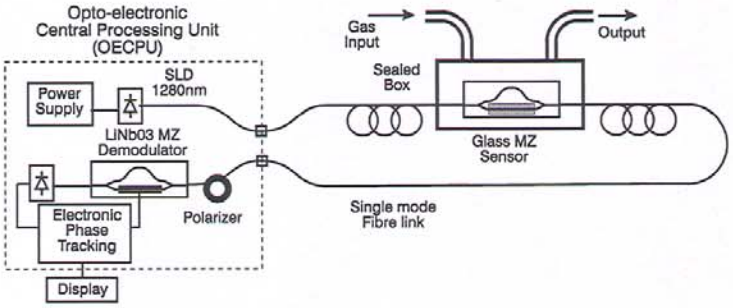

Fig. 1 Experimental setup of the remote gas sensor. The system is based on coherence modulation of light. It includes two integrated Mach-Zehnder devices. One is used as a sensor; the other one is used as an active demodulator. The measurement site is linked to the optoelectronic central processing unit by a single-mode optical fiber.

Under these conditions, no intensity modulation occurs at the output of the Mach-Zehnder and the transmitted optical power remains constant. The sensing process is the following. A thin layer of silicon dioxide is deposited at the surface of the waveguide interferometer. In this isolation layer, a window of length ℓ_s is opened over the sensing arm. The latter is then coated with an organic material. The polymer used is the dimethyl-phenyl-methyl-siloxane (DPMS), and behaves as a porous material able to absorb organic molecules, proportionally to their concentration in air. It results in a variation of the refractive index of the polymer superstrate proportionally to the concentration, the process being reversible. The mechanism linking the variation of the phase of the guided mode in the sensing arm to the refractive index variation is based on the interaction of the evanescent wave with the polymer.

The total optical path difference (OPD) of the interferometer, including the static path delay and the one depending on the concentration C of gas is thus given by:

$$\delta(C) = n_{eff}(L_2 - L_1) + \ell_s \frac{dn_{eff}}{dn_1}\frac{dn_1}{dC}C \tag{1}$$

Here, dn_1/dC is the coefficient of proportionality between the refractive index variation of the polymer and the concentration of gas. For DPMS, dn_1/dC is 4.1×10^{-2} for the vapor of ethanol and 1.3 10^{-2} for the butane gas. For our waveguide dn_{eff}/dn_1 was calculated to be 9×10^{-3}. The phase variation obtained with butane per millimeter of interaction length is expected to be 5.8 mrad/Vol%/mm. The order of magnitude of δ_o is of some tens to some hundred of microns. The variation of OPD under the influence of the gas concentration C is typically limited to some microns.

After transmission through the sensor, the optical signal propagates in the fiber and is demodulated in the OECPU where a second Mach-Zehnder interferometer featuring the same static OPD converts the variations of OPD in intensity variations. The static OPD of the demodulator introduced between the arms of length ℓ_1 and ℓ_2 of the Mach-Zehnder is given by $\delta_o = N_{eff}(\ell_2 - \ell_1)$, where N_{eff} is the effective index of the guided mode in the waveguide. If the OPD of the decoding interferometer remains constant, the signal detected by the photodetector is a cosine function of the variation of phase produced by the sensor.

In order to get a linear phase tracking, the decoding interferometer is realized in a lithium niobate crystal featuring an electrooptic effect. Thus, it becomes possible to control the OPD of the demodulator with an electrical voltage V applied to the electrodes deposited on the Mach-Zehnder arms. The orientation of the crystal, of the applied electric field and of the polarization of the light are chosen in order to get the highest electrooptic sensitivity. With a Z-cut crystal, the applied electric field and the polarization of the light (TM) being parallel to the Z-axis, the total OPD due to the decoding modulator and including the electrooptic effect is given by:

$$\delta(V) = n_e(\ell_2 - \ell_1) + \alpha V \tag{2}$$

with $\alpha = \frac{1}{2} n_e^3 r_{33} (\ell_2 + \ell_1) \frac{\eta}{d}$. Here $n_e = N_{eff}$ stands for the extraordinary refractive index of $LiNbO_3$ ($n_e \approx 2.14$), r_{33} is the highest electrooptic coefficient of the crystal (r_{33}=30.8 pm/V), η is the coefficient related to the overlap between the electrical and the optical fields ($\eta \approx 0.45$), d is the gap between the electrodes, and $(\ell_2 + \ell_1)$ is the total length of interaction for the electrodes considered here in a push-pull configuration. For instance, with a total length of electrodes of 30 mm, with a gap d =10 μm, and with a voltage ranging between –15 V and +15 V, the total accessible variation of OPD is about 6 μm. Thus, this value is comparable to the possible OPD variations of the sensing interferometer due to variations of gas concentration.

The optical signal transmitted by the demodulator and detected by the photodetector is proportional to:

$$I(C,V) = \frac{P_o}{4}\left[1 + \frac{1}{2}\cos\frac{2\pi}{\lambda_o}\left(\delta_g(C) - \delta_g(V)\right)\right] \tag{3}$$

The system behaves as if there was only one interferometer in the system, with one sensing arm on the measurement site and the other one in the OECPU. This is the key point of the system, since it is possible to keep the phase constant with the help of the voltage V, and to control and measure the phase variations of a sensor which can be distant of some hundred of meters up to some kilometers. The former aspect is of particular interest since this system does not require any electrical wires between the measurement site and the processing site. Hence, the phase remains constant and equal to 0, as long as the feedback voltage V verifies:

$$V = \frac{\ell_s}{\alpha} \frac{dn_{eff}}{dn_1} \frac{dn_1}{dC} C \tag{4}$$

This equation shows that it is possible to convert the concentration of gas into an electrical signal with an optical sensor system. Since the phase is measured directly, the system is insensitive to spurious intensity fluctuations, that may be caused on the transmission line.

2.2. Description of the integrated optics devices

Glass waveguide device

The Mach-Zehnder interferometric sensor integrated in glass is represented in Fig. 2. The device was realized using standards techniques: first a thin layer of aluminum was evaporated onto the glass sample. Using photolithography and chemical etching, the masking metal layer was opened to form stripes of 4μm wide. One arm of the Mach-Zehnder follows a straight line, while the other one is composed of four circle arcs with a bend radius R=50 mm. The geometrical difference of length between the arm is 58 μm.

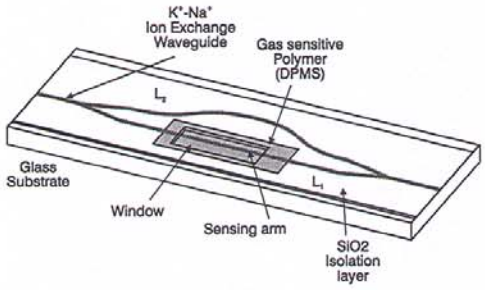

Fig. 2 Interferometric Mach-Zehnder sensor integrated in glass by K^+-Na^+ ion exchange process.

The waveguide is obtained by standard K^+-Na^+ ion exchange process in pure molten KNO_3 during 2-3 hours at 380°C, resulting in a single mode waveguide at 1300 nm-wavelength. The time of exchange was chosen in order to optimize the size of the optical field for an efficient coupling with a single mode fiber. The end faces were optically polished and a SiO_2 protecting layer was evaporated at the surface of the sample. A lift-off process was used to remove this protecting layer in order to open a window over the sensing arm. The length of the window corresponds to the length of the straight arm, i.e. ℓ_s=24 mm. The polymer DPMS was diluted in dichloromethane (9%) and then coated onto the sensing arm. The device was then pigtailed with single-mode fibers, resulting in -5 dB total insertion losses. The OPD was measured to be 91 μm.

Lithium niobate waveguide device

The lithium niobate demodulator depicted in Fig. 3 was realized using a conventional diffusion process. A 50 nm thick titanium layer is evaporated using an electron beam at the surface of a Z-cut crystal. The waveguide pattern is then reproduced by a photolithographic process and the layer is etched by $SiCl_4/Cl_2$ reactive ion etching. The width of the titanium stripes is 6μm. The geometrical difference of length between the arms is 38μm.

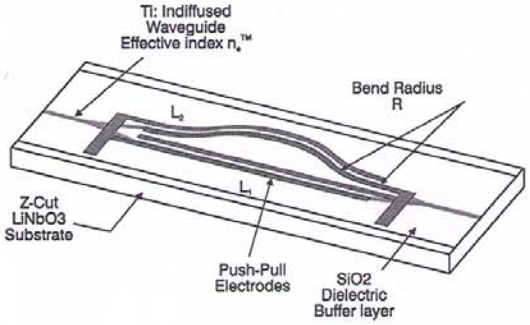

Fig. 3 Lithium niobate integrated optics Mach-Zehnder interferometer.

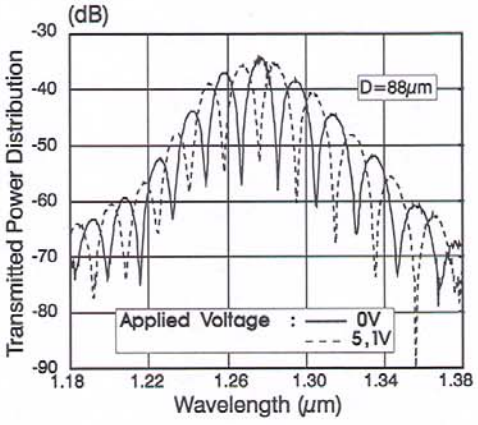

Fig. 4 Channeled spectrum transmitted by the lithium niobate Mach-Zehnder interferometer. The fringe spacing is 18.3nm. The curve in dotted line is obtained for an applied voltage of 5.1V corresponding to the half-wave voltage V_π.

The waveguides are then formed by high temperature diffusion (1050°C) of the titanium layer during 8 hours in a wet oxygen atmosphere. After diffusion, the end faces are polished and the

sample is coated with a silica dielectric buffer layer of thickness 180 nm, and with an aluminum layer. The electrodes are patterned in the aluminum layer by chemical etching. The waveguide pattern represented in Fig. 3 is designed in order to optimize the efficiency of the electrooptic interaction. The total insertion loss of the singlemode pigtailed device is better than -6dB.

The characteristics of the device were measured by spectral analysis. The transmission spectrum is represented in Fig. 4. The distance between adjacent peaks is here of $\Delta\lambda$=18.3 nm yielding a group static OPD introduced by the Mach-Zehnder of 89.5 μm. The sensor and the demodulator have their OPDs matched with an accuracy better than 2%. The curve in dotted line is in phase opposition with the one in solid line, corresponding to the application of the half-wave voltage V_π, which was measured here to be 5.1V, in good agreement with the predicted value that can be calculated from the parameters given in section **2**.

2.3. Experimental results

Testing and calibration were carried out by setting the sensor waveguide coated with the DPMS polymer into a hermetic package. Input and output pipes were used to inject a flow of air into the box with a known and previously calibrated gas concentration. The DPMS polymer has a good sensitivity to hexane methane and other gases. The results reported here are obtained with butane and vapor of ethanol.

The demodulation process and the optoelectronic feedback circuit which performs the linear tracking of the interferometric sensor signal were described in ref.7. The performances of the latter are the following: the output voltage range is –13V to +13V. This is equivalent to a total phase range of $\Delta\phi_{max}=5\pi$ rad. Due to noise, the smallest detectable phase shift (SDPS) is found to be $\Delta\phi_{min}$= 2mrad. The dynamic range is thus DR = $10\log(\Delta\phi_{max} / \Delta\phi_{min}) = 39$dB.

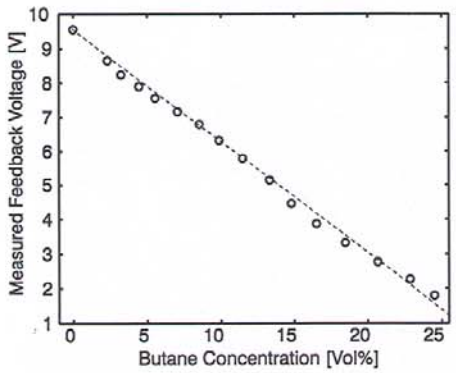

Fig. 5 Measured feedback bias voltage versus the concentration in air of the butane gas.

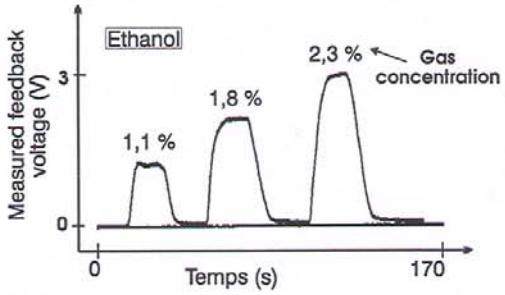

Fig. 6 Temporal response of the sensor system. Three pulses of vapor of ethanol are applied. The measured feedback voltage is plotted versus time in seconds.

Fig. 5 shows the results obtained with the measurement of concentration of butane gas in air. The gas concentration varies between 0 and 25% in volume. The feedback bias voltage variation is 8.1V and the resulting sensitivity can be assessed to be 8.3 mrad/%Vol/mm. This value can be merely compared with the theoretical value of 5.8mrad /Vol/% /mm. The absolute sensitivity for a 24 mm-long interaction is thus 0.2 rad/Vol %. Since the SDPS is 2mrad, the sensor has a resolution of gas concentration of 0.01% in volume. Figure 6 shows the response obtained when applying to the sensor three pulses of vapor of ethanol of calibrated concentrations equal to 1.1 %, 1.8 % and 2.3 % respectively. Here, the sensitivity is of 0.8 rad/Vol% and the response time of the sensor was measured to be 6 seconds.

3. Silicon pressure sensor

3.1 Description

The pressure sensor described here can be introduced in the processing system represented in Fig. 1. The device is depicted in Fig. 7, and consists of a (100) silicon substrate. An imbalanced Mach-Zehnder interferometer is integrated on the top face of the substrate. One interferometer arm is bent in order to introduce an optical path-delay. This bent arm is the reference arm. The straight arm is the sensing arm. Under the latter, three membranes of thickness e are micromachined from the back face of the substrate.

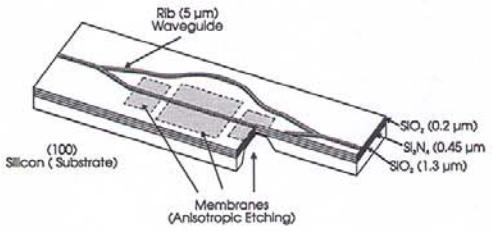

Fig. 7 Mach-Zehnder pressure sensor integrated in silicon. The waveguide is obtained with a silicon nitride layer set between two layers of silicon dioxide. Three membranes are etched under the sensing straight arm.

The fabrication of the device is carried out with the following steps: the substrate is first oxidized on both faces at high temperature. The resulting thickness of silica (SiO_2) is of 1.3 µm. A second layer of silicon nitride is deposited by PECVD on the top face of the substrate. The thickness of Si_3N_4 is of 0.45 µm. A third layer of silica of thickness 1.4 µm is deposited by PECVD. The silicon nitride layer of refractive index n_{Si3N4}=1.9 is the guiding layer, and the two layers of silica of refractive index n_{SiO2}=1.45 form the upper and lower cladding of the planar waveguide. The lateral confinement of the light is obtained by etching of a rib waveguide of width 5 µm in the upper silica layer, by using reactive ion etching (RIE). The thickness of etching is chosen in order to create a difference of effective index of 0.004 between the rib waveguide and the planar waveguide. The influence of the etching process becomes significant when the thickness of oxide is smaller than 0.5 µm. For larger values, the evanescent part of the guided wave does not propagate in air. The value of 0.004 for the effective index difference is obtained for a thickness of oxide of 0.2 µm. The thickness etched in the silica layer is thus 1.2 µm. The resulting effective index of the TE_{00} guided mode considered here is $n_{eff} \approx 1.725$.

The length of the straight Mach-Zehnder arm is L=20 mm. The deflection of the S-shape bent arm is 630 µm and the bent radius is 40 mm. The resulting length of the bent arm is thus 20.049 mm. The optical path-difference (OPD) introduced between the arms of the Mach-Zehnder interferometer is $\delta_{MZ}=n_{eff}(L_2-L_1)$=84.5 µm. As a broadband source will be used in this work, it is interesting to express the group optical path-delay which takes into account the chromatic dispersion of the

waveguide. The group effective index of the guided wave propagating in a highly confined (0.45 μm) waveguide is approximated by $n_g \approx 2$ at 1300 nm wavelength. This corresponds to a group optical path difference of δ_g=98 μm. After the waveguide fabrication, the membranes are realized by anisotropic etching in KOH from the back face of the crystal through the three windows opened in the oxide protecting layer chemically etched in buffered HF. The final thickness of the membranes is 21 μm. The membranes are of rectangular shape with a ratio b/a=2 between the length and the width. The sizes are b_1 = 2.61 mm and a_1 = 1.32 mm for the center membrane and b_2 = 1.93 mm and a_2 = 0.96 mm for the two side ones.

3.2. Principle of operation

The application of a pressure P under the membrane induces a deformation of the latter. The mechanical deformation of an elastic membrane can be described analytically. More particularly, the value of the deflection at the center of the membrane can be easily expressed and linked versus the pressure variation to the value of the variation of optical path difference by lengthening of the sensing arm. References 13 and 14 give the analytical expressions required to solve the problem.

We use the hypothesis, experimentally verified when using anisotropic etching, that the membranes are of rectangular shape of length b and width a. The thickness e is considered to be small compared to the sizes a and b. The thickness is assumed to be uniform and the four edges are assumed to be rigidly clamped to the substrate. The deformation is assumed to be perfectly elastic, which is the case with silicon membranes. We will neglect here for simplification the permanent stress produced by the first SiO_2 layer obtained by oxidation of the silicon substrate whose coefficient of dilatation is different from the one of the oxide layer. With these conditions, the pressure P can be expressed versus the deflection h_o at the center of the membrane by:

$$P = \frac{E}{1-\nu}\frac{e^3 h_o}{a^4}\left[\frac{1}{12\alpha(1+\nu)} + C\frac{h_o^2}{e^2}\right] \tag{5}$$

with: E=168200 MPa : silicon Young's modulus and ν=0.279 : Poisson's ratio α is a coefficient given by Timoshenko and Woinowsky-Krieger [13], depending on the ratio b/a. In our case b/a=2 and α=2.54 10^{-3}. Tabata[14] gave an analytical expression of the coefficient C: the Tabata coefficient calculated with $m=a/b$ =0.5 is equal to C=10.94. We can now assess the phase shift produced by a pressure P. Here we will only consider the phase variation produced by the lengthening of the sensing arm submitted to the deformation. As the waveguide is centered on the membrane, the elasto optical effects are negligible as demonstrated by other authors. The deflection is assumed to be small compared to the sizes of the membrane, and as the edges are rigidly clamped to the substrate, the slope of the deformation close to the edges is considered to be zero. One can deduce the excess length and thus the total optical phase variation. The latter is given for the three cascaded membranes by:

$$\Delta\phi(P) = \frac{2\pi}{\lambda} n_{eff}\,\Delta L(P) = \frac{\pi^3 n_{eff}}{2\lambda}\left[\frac{h_{o1}^2}{b_1} + 2\frac{h_{o2}^2}{b_2}\right] \tag{6}$$

The subscripts 1 and 2 stand for the large and the small membranes respectively. The non linear relationship of P with $\Delta\phi(P)$ is obtained by combining Eq.(5) and Eq.(6).

3.3. Experimental results

The device was designed, as previously discussed, to work in a coherence modulation scheme requiring a static optical path-difference to encode the information. In a first step, the main characterization was carried out by a spectral analysis of the light transmitted by the interferometer. Fig. 8 represents the results of the spectral analysis obtained as a pressure P=0 Bar then P=2.25 Bar

is applied to the membranes. This figure shows periodical transmission peaks in the spectrum of the source. This transmission peaks result from interferences at the output of the interferometer. The distance between adjacent peaks can be considered as the Free Spectral Range (FSR) of the filter: $FSR=\Delta\lambda=\lambda_o^2/\delta_g$. Measuring the FSR yields the value of the group OPD δ_g. Here $\Delta\lambda$ is measured to be 16.8 nm, corresponding to a static OPD δ_g=97.5 µm in good agreement with what was expected from the waveguide design (98 µm). The contrast of the fringes is 17 dB, yielding bend propagation losses in the bent arm of -2.2 dB.

In Fig. 8, one can measure the wavelength shift produced by the pressure variation. This wavelength shift can be linked to the variation of length of the waveguide arm.

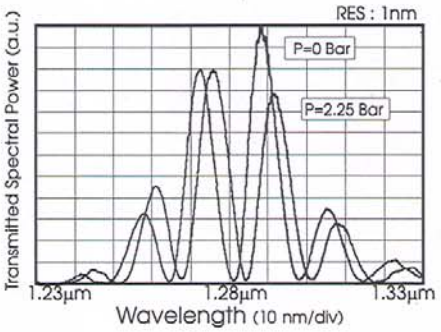

Fig. 8 Channeled spectrum transmitted by the imbalanced interferometer for an applied pressure of 0 and 2.25 Bar. The Free Spectral Range is 16.8 nm.

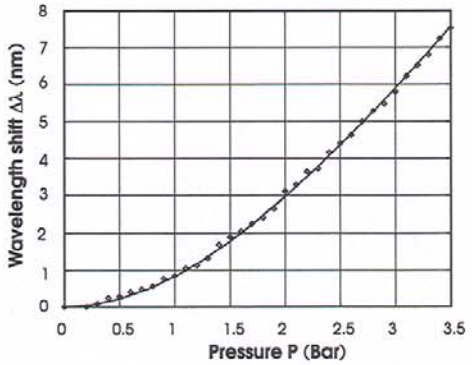

Fig. 9 Variation of the wavelength shift of the channeled spectrum versus the pressure variation. The solid line represents the curve obtained from the analytical model.

The wavelength shift of the channeled spectrum was measured between 0 and 3.5 Bar. Fig. 9 shows the variation of $d\lambda(P)$ against the pressure variation P. The curve in solid line is the analytical curve calculated from Eq.(5) and Eq.(6). It shows a good agreement with the experiments. The experimental curve of Fig.4 confirms that in the center of the membrane, the influence of the elasto-optic effects is much weaker than in the edges. The main contribution to the optical path variation comes mostly from the geometrical extension of the membrane. The accuracy of the measurement of the wavelength shift obtained in the experiment is about 0.1 nm yielding a relative accuracy in the determination of P of about $\Delta P/P$=1.4% around 3 Bar. This can be obviously improved by using of specially designed detection schemes [6,7].

4. Conclusions

We have discussed in a first time the feasibility of a gas sensor system based on coherence modulation of light for the remote interferometric measurement of gas concentration. The sensor uses an imbalanced interferometer integrated in glass and a demodulating interferometer integrated in lithium niobate. Sensitivity to the concentration of organic gas is achieved by the use of a layer of a specific polymer (DPMS) coated onto the sensor interferometer. The sensitivity thus obtained is 0.2 rad/Vol% for butane, and 0.8 rad/Vol% for ethanol vapor. The smallest detectabl e concentration of butane is 0.01% (0.0025% for ethanol) and the response time is 6 seconds. The observed resolution can certainly be increased by using an improved demodulation process.

In the second part, we demonstrated the feasibility of an optical pressure sensor based on the use of an imbalanced Mach-Zehnder interferometer integrated on silicon and associated with micro-machined membranes. Such an imbalanced interferometer compared to previous symmetrical interferometers allows simultaneously remote sensing and linear-phase read-out process at the output of the system, by coherence modulation scheme for instance or by spectral analysis. The latter system was used to measure the fringe displacement in a channeled spectrum produced by pressure variation ranging between 0 and 3.5 Bar, of the channeled spectrum transmitted by the device. The pressure required to produce a phase variation of π-rad is equal to 3.75 Bar. The description used introduces a non-linear deflection of the membrane versus the pressure applied. The experiments are in good agreement with the numerical and analytical models proposed here.

Acknowledgements

This work was supported by the *"GDR Microsystèmes"* programme of the CNRS and by the INCO/COPERNICUS programme of the European Community.

References

[1] Jackson D.A., Jones J.D.C., Opt. Acta **33**(12), 1469(1986).
[2] Brooks J.L., Wentworth R.H., Youngquist R.C., Tur M., Kim B.Y., Shaw H.J., J. Lightwave Technol. **3**, 1062(1985).
[3] Wentworth R.H., J. Lightwave Technol. **7**, 941(1989).
[4] Bløtekjaer K., Wentworth R.H. Shaw H.J., J. Lightwave Technol. **5**, 229(1987).
[5] Farhadiroushan M., Youngquist R.C., Opt. Lett. **15**(15), 786(1990).
[6] Singh H., Sirkis J.S., Andrews J., Pulfrey R., J. Lightwave Technol. **13**, 1772(1995).
[7] Porte H., Goedgebuer J.-P., Elflein W., Terras A., Ledeventec F., Butterlin N., IEEE J., Selected Topics in Quantum Electron. **2**(2), 319(1996).
[8] Ohkawa M., Izutsu M., Sueta T., Applied Optics **28**(23), 5153(1989).
[9] De Brabander G.N., Boyd J.T., Beheim G., IEEE Photonics Technology Letters **6**(5), 671(1994).
[10] De Brabander G.N., Beheim G., Boyd J.T., Appl. Opt. **37**(15), 3264(1998).
[11] Rehouma F., Elflein W., Persegol D., Kevorkian A., Clauss G., Benech P., Rimet R., Appl. Phys. Lett. **66**(12), 1461(1995).
[12] Luff B.J., Wilkinson J.S., Piehler J., Hollenbach U., Ingenhoff J., Fabricius N., J. Lightwave Technol. **16**(4), 583(1998).
[13] Timoshenko S., Woinowsky-Krieger S., Theory of plates and shells, Ch. XIII, McGraw-Hill Book Company, Inc. (1959).
[14] Tabata O., Kawahata K., Sugiyama S., Igarashi I., Sensors and Actuators **20**, 135(1989).